Constraining the contribution of aerobic nitrite oxidation to oxygen consumption in oceanic oxygen minimum zones

Beman, J.M.[1], S.M. Vargas[1], J.M. Wilson[1,2], E. Perez-Coronel[1], J.S. Karolewski[3], S. Vazquez[1], A. Yu[1], A.E. Cairo[1], M.E. White[2], I. Koester[2], L. I. Aluwihare[2], S.D. Wankel[3]

[1]Life and Environmental Sciences, University of California, Merced, Merced, CA, USA
[2]Scripps Institution of Oceanography, University of California, San Diego, CA, USA
[3]Marine Chemistry and Geochemistry, Woods Hole Oceanographic Institution, Woods Hole, MA, USA

Corresponding author: Prof. J. Michael Beman, Life and Environmental Sciences, University of California, Merced, 5200 North Lake Road, Merced, CA 95343, USA
E-mail: jmbeman@gmail.com
Phone: +1.650.823.7925

Author Contributions: J.M.B. designed the study and performed the research with S.M.V, J.M.W., E.P.C., J.S.K., S.V., A.Y., A.C., M.E.W. and I.K.; L.I.A. and S.D.W. contributed new analytical tools, and J.M.B. wrote the paper.

Competing Interest Statement: The authors have no competing interests.

This PDF file includes:
Main Text
Figures 1 to 5
Tables 1 to 2

Main Text Word Count: 5345
Reference Count: 63

Abstract

Oceanic oxygen minimum zones (OMZs) are globally significant sites of biogeochemical cycling where microorganisms deplete dissolved oxygen (DO) to concentrations <20 μM. Amid intense competition for DO in these metabolically challenging environments, aerobic nitrite oxidation may consume significant amounts of DO and help maintain low DO concentrations, but this remains unquantified. Using parallel measurements of oxygen consumption rates and ^{15}N-nitrite oxidation rates applied to both water column profiles and oxygen manipulation experiments, we show that the contribution of nitrite oxidation to overall DO consumption systematically increases as DO declines below 2 μM. Nitrite oxidation could account for all DO consumption only under DO concentrations <393 nM found in and below the secondary chlorophyll maximum. These patterns were consistent across sampling stations and experiments, reflecting coupling between nitrate reduction and nitrite-oxidizing *Nitrospina* with high oxygen affinity (based on isotopic and omic data). Collectively our results provide new insight into the contribution of nitrite oxidation to the maintenance and biogeochemical dynamics of OMZs.

Introduction

Aerobic nitrite oxidation is pervasive throughout much of the oceanic water column, playing a central role in deep ocean chemoautotrophy and carbon cycling[1,2], as well as in the oceanic nitrogen (N) cycle[3,4]. Nitrite oxidation rates are typically undetectable using $^{15}NO_2^-$ isotopic tracer in the sunlit euphotic zone, peak at the base of the euphotic zone, and subsequently decline with depth[5]. However, nitrite oxidation rate profiles deviate from this pattern in oceanic oxygen minimum zones (OMZs) that are depleted in dissolved oxygen (DO): rapid rates have been reported despite low DO concentrations[6-9], and nitrite oxidation itself may consume DO to low levels. OMZs are ultimately generated by high sinking fluxes of organic matter combined with reduced ventilation at depth, and are typically defined by DO concentrations <20 μM (ref. 10). Regions of the tropical oceans containing no measurable DO—termed anoxic marine zones (AMZs[11)]—are further distinguished by the accumulation of nitrite to comparatively high (>1 μM) concentrations[12]. These secondary nitrite maxima (SNM) result from anaerobic nitrate reduction to nitrite under low DO[11-13]. Accumulated nitrite may be subsequently reduced via denitrification and anaerobic ammonium oxidation—resulting in gaseous N loss[14]—or, alternatively, oxidized by NOB. Nitrite is therefore rapidly produced and consumed via multiple processes in OMZs, linking the oceans' N, carbon (C), and oxygen cycles.

Despite its centrality in OMZ biogeochemical cycles, nitrite oxidation is still poorly understood in these dynamic regions of the ocean. In particular, DO can be photosynthetically produced[15] or physically introduced to OMZs[12,16,17], requiring subsequent DO consumption in order to maintain the existence of the OMZ itself[4]. High rates of nitrite oxidation within OMZs suggest that marine nitrite-oxidizing bacteria potentially contribute to DO depletion, and therefore to the ultimate generation and maintenance of OMZs[4,6-9,15,17] . However, the contribution of nitrite oxidation to DO drawdown has not been directly quantified. While nitrite oxidation has been measured in several OMZs[6-9], oxygen consumption rate (OCR) measurements in OMZs are rare[16,18,19]. Yet simultaneous measurements are necessary to directly quantify the contribution of nitrite oxidation to oxygen consumption and to the maintenance of OMZs.

The central question addressed by our research is whether or not nitrite oxidation is a significant DO sink in OMZs, and, if so, over what range of DO concentrations does this occur? This has direct implications for our understanding of how OMZs form and expand[4,11], as well as associated consequences for C and N cycling and loss[3,14]. For example, an additional diagnostic

75 feature of AMZs is the presence of a secondary chlorophyll maximum (SCM) where distinct
76 ecotypes of the globally important cyanobacterium *Prochlorococcus* produce DO within low DO
77 waters[15,20,21]. Photosynthetic DO production is non-trivial, as production rates of up to ca. 100
78 nM-O_2 d^{-1} occur in the SCM—requiring corresponding DO consumption so that DO does not
79 accumulate[15]. SCM-based DO production can also overlap with nitrite supply via nitrate
80 reduction—which occurs at higher DO levels than previously thought, expanding the depth range
81 over which nitrate reduction and nitrite oxidation may interact[22,23]. However, the degree to
82 which nitrite oxidation (versus other processes) consumes DO in the SCM remains poorly
83 constrained[15]. Greater DO consumption via nitrite oxidation implies that less DO is used to
84 respire organic C, while the oxidation of nitrite precludes its further reduction to gaseous forms
85 of N[3,14].
86 Our understanding of how nitrite-oxidizing bacteria (NOB) oxidize nitrite in OMZs and
87 other low-DO habitats is also evolving. NOB gain energy by oxidizing nitrite to nitrate while
88 using DO as a terminal electron acceptor. NOB appear to have high affinity for DO (K_m values
89 of 778-900 nM DO or lower), allowing them to aerobically oxidize nitrite even at nanomolar
90 concentrations of DO[22,24]. Some NOB are also metabolically flexible[25], and perhaps able to
91 survive anaerobically through the use of alternative electron donors and acceptors[24,26,27].
92 Adaptations to low DO are evident in different NOB, and both *Nitrospina* and *Nitrococcus* may
93 contribute to oceanic nitrite oxidation varying degrees[26,28]. But although *in situ* nitrite oxidation
94 rates are typically highest under low DO (>100 nmol L^{-1} d^{-1})[6-9], experimental oxygen
95 manipulations show the opposite pattern: declining rates with declining DO[22]. This may be
96 explained by variations in genomic content among different NOB that allow them to occupy
97 distinct, highly-resolved DO niches throughout the water column[4,7,22,24,26]—including those that
98 occur from the edge (20 μM) to the core (<5 nM DO) of OMZs. High DO affinity among some
99 NOB also implies sensitivity to any DO introduced to incubations, and may partly explain some
100 of the elevated rates reported in OMZs. However, DO is rarely measured directly during nitrite
101 oxidation rate measurements, limiting our understanding of NOB affinity for DO and their
102 activity within OMZs. These details are essential to examine in the context of ocean
103 deoxygenation, as seemingly small variations in DO may have significant biogeochemical
104 implications if different ecotypes within different functional groups (such as nitrite oxidizers,

105 nitrate reducers, and organisms respiring organic matter aerobically) are adapted to specific DO
106 concentration ranges, and so display varying sensitivities to DO.
107 Here we address these open questions through parallel measurements of nitrite oxidation
108 and overall OCR in the oceans' largest OMZ, the eastern tropical North Pacific Ocean (ETNP).
109 Nitrite oxidation rate measurements (using $^{15}NO_2^-$), OCR measurements (using optical sensor
110 spots), and ammonia oxidation rate measurements (using $^{15}NH_4^+$) were made along depth
111 profiles at six stations in the ETNP, including three OMZ stations and three AMZ stations
112 (Figure 1). At each station, we sampled in the upper 100 m to capture the primary nitrite
113 maximum and an expected peak in nitrite oxidation rates at the base of the euphotic zone (EZ).
114 We then sampled a range of DO values (from 200 μM to the anoxic SNM at AMZ stations) to
115 quantify rate variations in response to vertical gradients in DO. How nitrite oxidation varies
116 from the OMZ edge to its anoxic core is critical to our understanding of ocean biogeochemical
117 cycles; we therefore conducted oxygen manipulation experiments and examined the response of
118 nitrite oxidation and OCR. Combined with natural abundance stable isotope data, 16S rRNA
119 sequencing, and metagenomes, we show that nitrite oxidation is a substantial—and occasionally
120 even dominant—sink for oxygen in the ETNP.
121
122 **Results**
123 *Nitrite oxidation rates in the ETNP*
124 We sampled six stations in the ETNP OMZ with DO concentrations <20 μM at depth (Figs 1 and
125 2). Three stations extending out from the coast of Mexico (Stations 1-3) were AMZ stations
126 with distinct SCMs and accumulations of nitrite in SNMs indicative of anaerobic N cycling
127 (Figure 2). We expected that these would be hotspots of nitrite oxidation given oxygen supply
128 via photosynthesis in the SCM overlapping with nitrite supply via nitrate reduction. Across all
129 stations and depths, we observed the highest nitrite oxidation rates at the AMZ stations (Fig. 2C,
130 G, and K). Station 1 is located nearest the coast and had a shallow OMZ at the time of our
131 sampling, with 20 μM DO at 28 m depth, and nitrite > 1 μM at 100 m (Fig. 2A). Chlorophyll
132 concentrations were also high in the upper water column (up to 5 mg m^{-3} at 20 m), with an SCM
133 spanning 70-125 m (Fig. 2B). Nitrite oxidation displayed a local maximum at the base of the EZ
134 at Station 1 (20-30 m), and then increased to higher levels (>100 nmol L^{-1} d^{-1}; Fig. 2C). This
135 increase at 100 and 125 m corresponded with the overlap between the bottom of the SCM and

136 the top of the SNM. Nitrite oxidation rates then reached higher values at 150 m within the SNM
137 at Station 1. Stations 2 and 3 displayed similar nitrite oxidation rate profiles to each other,
138 including elevated rates in the SCM (Fig. 2G and K). Nitrite oxidation rates were similar in
139 magnitude, and peak values at the base of the EZ and in the OMZ were also similar (69-96 nmol
140 L^{-1} d^{-1}). Depth patterns tracked oceanographic differences across the three AMZ stations, as the
141 depth of all features increased moving offshore from Station 1 to 2 to 3. For example, the SCM
142 extended from 105-155 m at Station 2, while nitrite concentrations began to increase below 100
143 m; nitrite oxidation rates were elevated at 140 m and declined slightly with increasing depth (Fig.
144 2E-G). At Station 3, the SCM (120-180 m) and SNM (>140 m) depths were deeper, and nitrite
145 oxidation rates increased from 100 to 200 m (Fig. 2I-K).
146 In contrast to these three AMZ stations (Stations 1-3), rate profiles at Stations 4-6 showed
147 peaks at the base of the EZ followed by decreases with depth, and lacked a pronounced rate
148 increase within the OMZ (Supplementary Figure 1). Parallel measurements of ammonia
149 oxidation rates also showed this type of pattern at all stations (Supplementary Figure 1).
150 Subsurface maxima in ammonia oxidation tracked variations in the EZ across all six stations, but
151 rates were not elevated in OMZ/AMZ waters—again contrasting with nitrite oxidation rate
152 profiles at the AMZ stations. These data accord with earlier work in OMZs showing contrasting
153 ammonia and nitrite oxidation rate profiles, and particularly high rates of nitrite oxidation in
154 OMZ waters[6-8,29-31].
155 Initial DO concentrations for these measurements closely matched *in situ* values above
156 the SCM (where DO concentrations are higher), and starting DO ranged from 260-1500 nM for
157 measurements in and below the SCM. These DO concentrations are generally lower than those
158 used for previous nitrite oxidation rate measurements in OMZs[6,9], but similar to work examining
159 the oxygen affinity of nitrite oxidation[22] and overall oxygen consumption[16,19]. Elevated nitrite
160 oxidation in the limited number of samples (n=5) collected below the SCM (> 125 m at Station
161 1, >155 m at Station 2, and >180 m at Station 3)—where little to no DO is typically available—
162 should be considered potential rates and could have a number of possible explanations discussed
163 below. Within the SCM, our data support the idea that nitrite oxidation contributes to 'cryptic'
164 oxygen cycling[15]—i.e., that DO produced via oxygenic photosynthesis is rapidly consumed.
165
166 *Oxygen consumption via nitrite oxidation*

167 We determined the contribution of nitrite oxidation to overall oxygen consumption via parallel
168 measurements of oxygen consumption rates (OCR) using *in situ* optical sensor spots—which are
169 non-invasive, provide nearly identical results as other low-level measurement approaches[32], are
170 the only effective means of achieving of substantial replication, and for which sensitivity
171 increases as DO decreases[32,33]. Decreases in DO were measured in both nitrite and ammonia
172 oxidation rate sample bottles, as well as in three additional replicates, to leverage statistical
173 power for increased sensitivity to low-level DO consumption (see Materials and Methods).
174 Water column OCR profiles at all stations showed exponential declines with depth and
175 decreasing DO concentrations (Fig. 2D, H, and L and Supplementary Figure 1). Rates were
176 highest in the upper water column, and declined sharply within the upper portion of the OMZ
177 above the SCM. The majority of measurements within the SCM—where DO may be produced
178 via photosynthesis—were 100s of nmol L^{-1} d^{-1}, with an overall range of 160-1380 nmol L^{-1} d^{-1}.
179 Below the SCM, DO would be available more rarely (e.g., ref. 16), and OCR measurements
180 represent potential rates should oxygen be supplied; OCR ranged from 120-390 nmol L^{-1} d^{-1}.
181 OCR also tracked variations in DO across stations, with progressively steeper declines in OCR
182 with depth from Station 6 through Station 1.
183 These OCR results are similar to the limited previous measurements that have been
184 conducted in OMZ regions, with some key differences. In particular, they are consistent with
185 previous measurements of rapid DO consumption in the SCM, with OCR rates ranging from
186 482-1,520 nmol-O_2 L^{-1} d^{-1} in the ETSP, and from 55-418 nmol-O_2 L^{-1} d^{-1} in the ETNP[15]. Earlier
187 OCR measurements conducted in the ETNP near Stations 1 and 3 (across a wide range of DO
188 values) likewise ranged from 420-828 nmol L^{-1} d^{-1} in the SCM near Station 1, and from 101-269
189 nmol L^{-1} d^{-1} in the SCM near Station 3 (ref. 16). Above the SCM, previous OCR measurements
190 in the ETNP spanned 2,260 to 662 nmol L^{-1} d^{-1} from the EZ to the edge of the OMZ; these
191 values are lower than our measurements at 44 and 67 m depth at Station 2, but in line with our
192 remaining measurements above the SCM. OCR reached 1610 nmol L^{-1} d^{-1} in the SCM in
193 Namibian shelf waters, and 200-400 nmol L^{-1} d^{-1} in the SCM off Peru[18]. Kalvelage et al.[18]
194 furthermore observed sharp decreases with depth in the ETSP, with rates declining from >1000
195 nmol L^{-1} d^{-1} above the SCM.
196 This pattern of declining OCR with increasing depth and decreasing DO was also evident
197 in our dataset, and contrasted with that of nitrite oxidation rates, which were notably elevated in

198 the SCM at the AMZ stations (Fig. 2). We directly compared nitrite oxidation rates with OCR,
199 assuming that each mole of nitrite is oxidized using ½ mole of O_2 (ref. 5). We found that nitrite
200 oxidation systematically increased as a proportion of overall OCR at lower DO levels (Figure 3A
201 and B). Nitrite oxidation was responsible for up to 69% of OCR at Station 1, although most
202 values were closer to 10-40% at Stations 2 and 3 (Fig. 3A and B). In contrast, ammonia
203 oxidation contributed < 5% of oxygen consumption in the OMZ (Supplementary Figure 1).
204 Overall, these data demonstrate consistent patterns in the contribution of nitrite oxidation to
205 OCR, as the proportion of DO consumed by nitrite oxidation increased at progressively lower
206 DO concentrations across multiple stations.
207
208 *Effects of oxygen manipulation experiments on nitrite oxidation and OCR*
209 We corroborated these observations by experimentally manipulating DO concentrations to
210 measure the response of OCR, as well as $^{15}NO_2^-$ nitrite oxidation rates, to changing DO (Figure
211 4). To examine responses of different assemblages in different depth regions, we conducted
212 experiments on the edge of the OMZ at Stations 2-4, in the SCM at Stations 2 and 3, and in the
213 SNM at Station 3 and an additional sampling Station 3.5 (Table 1). (We could not conduct
214 additional experiments at Stations 1 and 2 owing to a hurricane in the region at the time of
215 sampling in 2018, and added Station 3.5 as a result.) Oxygen manipulations were designed to
216 quantify OCR and nitrite oxidation across the full spectrum of DO concentrations that occur
217 from the OMZ edge to its core—rather than solely probing their lower limits—in order to
218 constrain rate responses to changing DO within OMZs.
219 Oxygen manipulation experiments were consistent with water column profiles and
220 provide additional evidence that nitrite oxidation can be a substantial oxygen sink. In all
221 experiments, we found that OCR declined with experimentally decreased DO (Fig. 4). These
222 declines in OCR were particularly steep below 1-2 μM DO across different experiments. For the
223 SCM and SNM experiments, DO concentrations >1 μM are obviously higher than expected to
224 occur *in situ* (Table 1), but these concentrations were included for comparison across
225 experiments and with earlier studies[9,15]; OCR measurements for SCM and SNM samples
226 conducted at DO concentrations >100s of nM therefore represent potential rates. For OMZ edge
227 samples, OCR values in the μM range were higher than observed in profiles—most likely due to
228 the effects of bubbling[19], which could physically break down organic matter present in higher

concentrations at these depths (Table 1). Throughout all experiments, rate magnitudes in the 100s of nM DO concentration range (11-820 nmol L^{-1} d^{-1}) were similar to profile measurements (Fig. 2), as well as to previous measurements in OMZs[15,16,18,19] (see above).

DO concentrations were also continuously monitored in a subset of experimental bottles, and DO consumption was consistently linear (see Methods). The few exceptions occurred in several experiments conducted at DO concentrations <235 nM; in these experiments, OCR declined as DO was consumed over time (Supplementary Figure 2). These observations are consistent with Tiano et al.[16] and allowed us to calculate the low-level DO affinity of the community (following ref. 16), in addition to overall values based on variations across all experimental incubations (following ref. 19; Supplementary Note 1). However, we note that both reflect mixed assemblages of microorganisms that use DO to oxidize a variety of substrates (Supplementary Note 1). These substrates can include nitrite, as well as different forms of organic matter, reduced sulfur compounds, and possibly methane[34]. Low-level results were consistent with previous observations indicating high affinity for DO (K_m ranged from 53-127 nM DO), and, importantly, all data demonstrate that OCR decreases as DO decreases (Supplementary Note 1, Table 1).

In line with earlier work[22,24], nitrite oxidation rates also declined in response to decreasing DO in most of our experiments (Fig. 4). However, nitrite oxidation rates were less sensitive to declining DO than OCR (Supplementary Note 2). Nitrite oxidation was therefore responsible for progressively higher proportions of overall OCR as DO was experimentally decreased (Fig. 3C). In fact, we found that 97% of OCR in the SCM at Station 2 could be explained by measured nitrite oxidation rates—indicating that nitrite oxidation alone can sustain all DO consumption at DO concentrations just below 393 nM. However, most values were closer to 10-20%, and this contribution was obviously variable across experiments: while our experiment in the SCM at Station 2 showed that nitrite oxidation can consume all available DO (Fig. 4B), the experiment with 20 μM [DO] water at Station 2 suggests that, even at low DO levels, nitrite oxidation would not consume all DO (Fig. 4A). This highlights the fact that nitrite oxidation is unlikely to be dominant on the edge of the OMZ due to higher DO and organic matter concentrations, along with lower nitrite concentrations, compared with the SCM (Figs. 2 and 3, Table 1). Overall, patterns in experiments were notably similar to results from rate profiles: both showed increases in the contribution of nitrite oxidation to DO consumption below

260 2 μM DO, both followed significant power-law relationships (experimental r^2=0.40, P<0.0005;
261 profiles r^2=0.51, P<0.0001), and both displayed similar values (Fig. 3B and C).
262 These data tie together multiple aspects of OMZ biogeochemistry into a coherent picture.
263 Although nitrite oxidation rates decline as DO is experimentally decreased at individual depths—
264 and so with particular assemblages of NOB—different depths/assemblages display different
265 properties (Fig. 4 and Supplementary Note 2). More importantly, this decline is always less
266 severe for nitrite oxidation than for overall OCR (Figs. 2-4). NOB are therefore effective at
267 scavenging DO (Figs. 3 and 4; ref. 15), and the concentration range over which they become
268 increasingly important (0.2-1 μM DO) matches model predictions involving a nitrogen-oxygen
269 feedback loop in OMZs driven by oxygen depletion via nitrite oxidation[17].
270
271 *Isotopic, 16S rRNA, and metagenomic constraints on nitrite oxidation*
272 To further verify our findings, we applied natural abundance stable isotope measurements, 16S
273 rRNA sequencing, and metagenome sequencing to water samples and nucleic acid samples
274 collected in parallel with nitrite oxidation rate measurements (Figure 5). The dual N and O
275 isotopic composition of dissolved nitrate ($\delta^{15}N$ and $\delta^{18}O$, respectively; Supplementary Figure 3)
276 is thought to provide an effective constraint on nitrite oxidation under low DO conditions due to
277 isotopic 'overprinting' by nitrite oxidation[35,36]. While the respiratory reduction of nitrate
278 (denitrification) leads to equal 1:1 increases in $\delta^{15}N$ and $\delta^{18}O$ (refs. 37, 38), deviations in 1:1
279 N:O isotope behavior arise from a decoupling of the N and O systems. These deviations are
280 widely interpreted as reflecting cryptic re-oxidation of nitrite under low DO, where the reduction
281 of nitrate to nitrite removes an O atom, and the subsequent re-oxidation of nitrite to nitrate
282 appends a new O atom derived from ambient water[39,40]. Deviations from the 1:1 relationship are
283 represented via Δ(15,18) values[41], where more negative values represent larger departures from
284 the 1:1 relationship.
285 At Stations 1-3, dual nitrate isotope values exhibited non-linear trends (Figure 5B and
286 Supplementary Figure 4) that are consistent with isotopic overprinting by nitrite oxidation[35,36].
287 Δ(15,18) values were lowest (i.e., deviations were largest) at 50-150 m at Station 1, 100-140 m at
288 Station 2, and 110-160 m at Station 3. The lower portions of these depth ranges overlapped with
289 the upper portion of the SCM (75-125 m, 105-155 m, and 120-180 m, respectively) and tracked
290 depth variations between stations. Peak deviations at Stations 1 and 2 were just above the SCM

291 (75 and 100 m), while the peak at Station 3 corresponded closely with the SCM (140 m).
292 Throughout these ETNP OMZ sites, our nitrate isotope data are consistent with previous
293 observations and interpretations of rapid recycling between nitrate and nitrite[35,41,42], ultimately
294 evidenced by isotopic overprinting of the nitrate reduction signal by nitrite oxidation.
295 16S rRNA gene and transcript sequencing revealed a similar pattern to rate profiles,
296 experiments, and isotopic data, while also enabling identification of NOB that are abundant and
297 active in the ETNP OMZ. Based on DNA, *Nitrospina* 16S rRNA amplicon sequence variants
298 (ASVs; ref. 43) comprised up to 3.4-5.4% of all ASVs at Stations 1-3 (Fig. 5C), and relative
299 abundances were consistent with biogeochemical data. Abundances and isotopic deviations were
300 well-correlated (r^2=0.70-0.84, P<0.05) at Stations 1 and 3, for instance, while abundances
301 correlated with nitrite oxidation rates (r^2=0.20-0.46, P<0.05) at Stations 2 and 3. Patterns
302 observed for DNA samples were accentuated for RNA, with discrete peaks in 16S rRNA
303 transcripts generally occurring at deeper depths (Fig. 5D). *Nitrospina* 16S rRNA peaked at 125
304 m at Sta 1 (1.8% of all 16S rRNA transcripts; with an additional upper water column peak at 50
305 m), 140 m at Station 2 (3.2%), and particularly 140-180 m at Station 3 (1.6-7.1%). All of these
306 depths lie within the SCM at each station. Although 20 *Nitrospina* ASVs were identified, three
307 were dominant (each >1% of all ASVs, together constituting 72-100% of all *Nitrospina* 16S
308 rRNA gene sequences and transcripts). One of these ASVs was found only in OMZ samples at
309 Stations 1-3, and was not detected above the OMZ, nor at Stations 4 and 5 (Supplementary
310 Figure 5). This was also the lone ASV observed in the OMZ at Station 3, where *Nitrospina* were
311 most active based on their comparatively high percentages of all 16S rRNA transcripts. In
312 contrast, no *Nitrococcus* ASVs and only one low-abundance *Nitrospira* ASV were identified out
313 of >11,000 ASVs and >3.5 million 16S sequences from 73 DNA and 73 RNA samples. In line
314 with earlier work in the ETNP[7,26], other OMZs[6,44], and the variations in DO affinity observed
315 across oxygen manipulation experiments (Fig. 4), these results indicate that particular *Nitrospina*
316 ecotypes—and one ASV in particular—are significant for low-oxygen nitrite oxidation, while
317 other ASVs may be more important at different depths and DO concentrations.
318 To validate the genetic potential for nitrite oxidation by *Nitrospina* under low DO
319 concentrations, we sequenced metagenomes collected on the OMZ edge, at the SCM, and within
320 the OMZ core at Stations 1, 2, and 3. Nitrite oxidoreductase (*nxr*) genes from *Nitrospina* were
321 prevalent at all stations and depths, establishing the genomic potential for nitrite oxidation

322 throughout the ETNP OMZ (Table 2). *nxr* and all *Nitrospina* genes were most abundant in the
323 SCM, consistent with a range of omic data showing maximal *Nitrospina* gene or enzyme
324 abundances in the upper portion of AMZs[2,7,15,26]. In addition, multiple high-affinity cytochrome
325 C oxidase genes from *Nitrospina* were present in all samples—indicating that *Nitrospina* are
326 capable of consuming DO at the low concentrations found within the OMZ. These genes were
327 more common in SCM and SNM metagenomes than at the OMZ edge, consistent with
328 *Nitrospina* ecotype distributions, and with the lower DO concentrations found in the SCM and
329 SNM (Table 2). Cytochrome *bd*-type oxidase genes from *Nitrospina* were also detected in all
330 metagenomes except the OMZ edge sample at Station 1, although these lack quinol binding sites
331 and may not function as canonical oxidases[26,45]. Sun et al.[26] also suggested that chlorite
332 dismutase genes may be relevant for anaerobic metabolism in *Nitrospina*, and these were present
333 in all metagenomes (Supplementary Table 1). We also recovered formate dehydrogenase and
334 nitrate reductase genes indicative of anaerobic metabolism in *Nitrospina*[25] (Supplementary Table
335 1). Both of these genes were absent from OMZ edge metagenomes at Stations 1 and 2, showing
336 higher relative abundances in the SCM, and especially the SNM. *Nitrospina*-derived nitrate
337 reductase genes were present at similar levels as nitrite oxidoreductase in the SNM, while less
338 common in the SCM (Supplementary Table 1). Finally, *Prochlorococcus* genes were prevalent
339 from the OMZ edge to core, and especially within the SCM, supporting the idea that oxygenic
340 photosynthesis and cryptic oxygen cycling occur throughout the ETNP OMZ (Table 2). Overall,
341 metagenomic data are consistent with experimental data and 16S data, and indicate *Nitrospina*
342 are tightly tuned to DO concentrations in the ETNP.
343
344 **Discussion**
345 Assembled together, our results provide a comprehensive view of nitrite oxidation and its
346 contribution to oxygen consumption in the ocean's largest OMZ. Rate measurements, oxygen
347 manipulation experiments, stable isotopic data, and molecular data all converge on the fact that
348 nitrite oxidation is active from the base of the euphotic zone into the OMZ. Nitrite oxidation was
349 particularly significant within the SCM at Stations 1-3: nitrite oxidation rates were elevated (Fig.
350 2), isotopic overprinting of nitrate by nitrite oxidation was evident (Fig. 5B and Supplementary
351 Figure 4), and *Nitrospina* were abundant and active (Fig. 5C and D). All of these data tracked
352 systematic progression in the depth of the SCM across stations (Fig. 2), and indicate that nitrite

353 oxidation is important for DO utilization in the SCM. Based on rate profiles, nitrite oxidation
354 ranged from 10-47% of OCR in the SCM (Fig. 3B), while experiments indicate maximum
355 percentages of 13-97% (Fig. 3C). Stations 4-6—which lack a SCM and SNM—provide a
356 notable contrast, as do ammonia oxidation rate profiles (Supplementary Figure 1).
357 Peaks in the magnitude of departure from a 1:1 nitrate reduction signal (e.g., isotopic
358 overprinting by nitrite oxidation), and in *Nitrospina* ASV abundances, further indicate that nitrite
359 oxidation is active above and below the SCM (Fig. 5). At Stations 2 and 3, nitrite oxidation rates
360 above the SCM were similar to rates deeper in the water column, while Station 1 showed a rate
361 increase within the AMZ (Fig. 2). In OMZs/AMZs, DO may be photosynthetically produced in
362 the SCM[15,46] or introduced through physical mixing[12,16,46], but both of these DO sources would
363 be less significant below the SCM. Instead, the introduction of DO during sample manipulation
364 effectively measures the potential for oxygen consumption in samples collected below the SCM.
365 Short of conducting *in situ* incubations, such DO contamination is essentially unavoidable, and is
366 the reason that we also performed oxygen manipulation experiments (Fig. 4)—which also have
367 limitations[19]. In line with earlier work in OMZs facing these same challenges[16,18], oxygen
368 consumption potential was significant even below the SCM. Most importantly, inclusion of DO
369 sensor spots in all bottles allowed us to directly measure DO in every incubation, and therefore
370 to quantify nitrite oxidation and OCR as a function of DO across all profiles and experiments.
371 Patterns in OCR and nitrite oxidation were notably consistent between profiles and experiments
372 (Fig. 3B and 3C). This similarity indicates that—independent of methodology—nitrite oxidation
373 increases in relative importance below 2 μM DO.
374 To make our findings widely relevant to current and emerging OMZ regions, we
375 examined the full range of DO concentrations found in OMZs, rather than in the AMZ
376 exclusively. However, consistent with isotopic data, we found that *Nitrospina* 16S rRNA
377 transcripts increased in relative abundance within the AMZ (Fig. 5). RNA samples were
378 collected from the CTD rosette and rapidly filtered, so if these data capture a response to oxygen
379 exposure, this response is exceptionally rapid and consistent. Alternatively, these data indicate
380 that *Nitrospina* are active within the AMZ. One possibility is that *Nitrospina* survive
381 anaerobically for periods of time until provided DO[25]. Oxygen-evolving mechanisms from
382 nitrite have also been proposed for anaerobic methane-oxidizing bacteria[47] that are active in
383 OMZs[48]. The presence of *Prochlorococcus* below the SCM may allow low-level DO production

384 via oxygenic photosynthesis[46] (Table 2). Finally, Tiano et al.[16] previously detected DO at 500 m
385 depth within the core of the ETNP AMZ. This is substantially deeper than our experiments and
386 well below the SCM (Fig. 2)—suggesting that DO can be periodically introduced even deep
387 within the AMZ. Regardless of the mechanism, isotopic data and 16S rRNA data suggest that
388 transient nitrite oxidation coupled to nitrate reduction occurs below the SCM[17].
389 However, our primary focus was on oxygen consumption via nitrite oxidation and its
390 implications for the formation, maintenance, and expansion of OMZs. Two clear and
391 remarkably consistent patterns emerged from both water column profiles and oxygen
392 manipulation experiments: (i) overall OCR declined with decreasing DO in profiles and
393 experiments (Figs. 2C and 4), while (ii) nitrite oxidation increased as a proportion of OCR as DO
394 declined in both profiles and experiments (Fig. 3B and C). Nitrite oxidation was significant
395 throughout the OMZ and experiments, but increased in relative importance below 2 μM DO—
396 typically ranging from 10-40% of OCR—and was only dominant (>50% OCR) at low DO
397 concentrations (Table 1). For example, nitrite oxidation consumed nearly all DO produced in the
398 SCM experiment at Station 2 (Fig. 3C). Variation in the proportion of overall OCR attributable
399 to nitrite oxidation could reflect fluctuations through time[17], as well as differences in substrate
400 availabilities and affinities relative to DO for different processes consuming DO. Other than
401 nitrite oxidation, aerobic respiration of organic matter is most significant for OCR given relative
402 substrate concentrations (organic C > CH_4 or reduced S compounds; refs. 48–50), as well as high
403 affinities for DO among heterotrophic bacteria[51-53]. Our data indicate that aerobic heterotrophic
404 respiration is likely the dominant DO-consuming process from the edge of the OMZ (20 μM
405 DO) until OCR declines precipitously (Fig. 4 and Table 1).
406 Many aerobic heterotrophs are also facultatively anaerobic, switching to nitrate reduction
407 under low DO[13,54]. Along with a substrate-driven decline in aerobic respiration rates with
408 decreasing DO, this shift to nitrate reduction likely explains the steep declines in OCR observed
409 in our experimental data (Fig. 4). Production of nitrite from nitrate reduction also provides a
410 needed substrate for nitrite oxidation, and is consistent with isotopic data (Fig. 5B and
411 Supplementary Figure 4). We suggest that such cryptic nitrite/nitrate cycling explains the
412 adaptations of particular *Nitrospina* bacteria to AMZs: although these are low-DO environments,
413 they are also high-nitrite environments, representing a trade-off in the availability of electron
414 donor and acceptor. The fact that nitrite oxidation rates increase with increasing nitrite into the

415 micromolar range[9], and that nitrate is reduced at similar rates[55], provides additional support for
416 this idea. Our results further indicate that nitrite oxidation is carried out by just a few *Nitrospina*
417 ASVs under these conditions (Supplementary Figure 5)—in contrast with the diversity of other
418 microbial groups that may be involved in overall oxygen consumption[4,56]. These *Nitrospina* are
419 disproportionately biogeochemically important given their roles in DO consumption and
420 regeneration of nitrate, which precludes its further reduction. For these organisms, the costs of
421 life at low DO are offset by the advantages of persistently elevated nitrite concentrations.
422 At the same time, efficient scavenging of DO by *Nitrospina* can maintain DO at low
423 levels favorable for nitrate reduction[17,57]. This represents a form of biogeochemical symbiosis,
424 in that microorganisms performing nitrite oxidation and nitrate reduction mutually benefit from
425 their biogeochemical interaction. Rate profiles, oxygen manipulation experiments, natural
426 abundance measurements, 16S rRNA sequencing, and metagenomic data all favor this idea: the
427 proportion of DO consumed by nitrite oxidation increased at progressively lower DO
428 concentrations in both profiles and experiments (Fig. 3B and C); isotopic anomalies are
429 indicative of coupled nitrite oxidation and nitrate reduction (Figs. 5B and Supplementary Figure
430 4); and the low-oxygen adaptations of particular *Nitrospina* support high abundances and activity
431 (Table 2, Fig. 5C and D, Supplementary Figure 5). These data also provide multiple lines of
432 direct evidence that verify model results showing co-existence of nitrite oxidation and nitrate
433 reduction emerging below ~1 μM DO (refs. 17, 57). By placing entirely new bounds on the
434 contribution of nitrite oxidation to DO consumption, we resolve the niche of nitrite-oxidizing
435 *Nitrospina* within OMZs, quantify their contributions to coupled oxygen and nitrogen cycling,
436 and convincingly establish that nitrite oxidation is pivotal in the maintenance and
437 biogeochemical dynamics of these important regions of the ocean.
438
439 **Materials and Methods**
440 **Sample Collection.** Samples were collected in April 2017 and June 2018 aboard the *R/V*
441 *Oceanus*. At each station, conductivity/salinity, temperature, depth, pressure, chlorophyll
442 fluorescence, and photosynthetically active radiation (PAR) were measured by a SeaBird SBE-
443 9plus CTD, SBE-3F temperature sensor, SBE-43 DO sensor, WetLabs ECO-FLR Fluorometer,
444 and Biospherical QCP2200 PAR sensor. Initial casts were used to measure DO and nutrient
445 profiles to guide subsequent sampling. Nutrient samples were analyzed for NH_4^+ and NO_2^-

446 aboard the ship, with additional shore-based analyses of combined NO_3^-+NO_2^- and PO_4^{3-} at the
447 University of California Santa Barbara Marine Science Institute Analytical Lab (Supplementary
448 Materials and Methods).
449 At all stations, water samples were collected in the upper 100 m to capture variation in
450 the upper water column, and we then sampled across a range of DO levels and nitrite levels to
451 capture variation in the OMZ (Supplementary Table 2). Samples were collected at 200, 100, 50,
452 20, 10, 5, and 1 μM [DO] at all stations. Because the OMZ is shallower and more intense
453 moving south and nearshore in the ETNP (Fig. 1), these DO levels can occur within the upper
454 100 m, such that upper 100 m and DO-based sampling overlapped. This overlap was greater at
455 Station 1, followed by 2 and 3. At these AMZ stations, samples were also collected at three
456 depths below the 1 μM [DO] level of the CTD, within the SNM (Supplementary Table 2).
457 Experiments were conducted for 24 hours in the dark in a cold van adjusted to ambient
458 temperature, with separate incubations (and therefore temperatures) conducted for samples from
459 the upper 100 m, for oxygen/nitrite-based sampling, and for oxygen manipulation experiments at
460 each station.
461
462 **OCR Measurements and Oxygen Manipulations**. Two types of sensor spots were used to
463 measure OCR and manipulate DO, one with a wider range and detection limit of 100 nM (Fibox,
464 Loligo Systems, Viborg, Denmark), as well as trace-level spots with a detection limit of 10 nM
465 (FireSting, Pyroscience, Aachen, Germany). Loligo sensor spots were used in 2017 for water
466 column profiles given the wider DO range, while FireSting trace-level spots were used in 2018 to
467 establish oxygen manipulation experiments and measure OCR within them. Optical sensors
468 were calibrated using DO-saturated water and sodium sulfite-saturated and He-purged water. On
469 the upper end, Fibox sensor spot DO measurements were highly correlated with CTD DO values
470 (r^2=0.996, slope=0.997, P<0.00001) for [DO] > 1 μM. On the lower end, we regularly checked
471 the '0 nM' concentration with repeated measurements of sodium sulfite-saturated water and He-
472 purged water, and our lowest values measured in experiments were below the detection limit (10
473 nM) of the FireSting. In both profiles and experiments, OCR was measured by the decrease in
474 DO over the course of experiments[32,58].
475 Water column profiles of OCR were measured using 5 replicates at each depth, including
476 one each with tracer level (5-10% *in situ* concentration measured at sea) addition of $^{15}NH_4^+$ or

477 $^{15}NO_2^-$ to measure ammonia/nitrite oxidation (see below). Loligo sensor spots were attached to
478 the inside of 300 mL Wheaton BOD glass bottles using silicone glue. At sea, bottles were filled
479 to at least three times overflowing via slow laminar flow, were rapidly capped and transferred to
480 the cold van, and initial DO measurements were made. DO was measured subsequently at 10-14
481 hours, and at the end of the 20-24 hour incubations. The majority of OCR rate values calculated
482 at these 10-14 hour and 20-24 hour measurement time points were highly correlated with each
483 other (r^2= 0.968-0.995; slopes=1.06-1.19; all P<0.0001 across different stations), indicating that
484 OCR did not accelerate or decrease substantially over the course of the incubations. The only
485 exceptions were three sampling depths from station 3 (77, 87, 97 m) showing nonlinearity, and
486 so we report data from duplicate OCR measurements conducted at similar depths (75, 88, 100 m)
487 during the previous 24 hour period (when nitrite oxidation rates were not measured in tandem).
488 After incubation, endpoint DO measurements were made, and then 50 mL samples from relevant
489 bottles were frozen for nitrite and ammonia oxidation rate measurements.
490 Oxygen manipulation experiments were conducted in 500 mL serum bottles with
491 attached FireSting sensor spots. We conducted a total of seven experiments, with experiments
492 on the OMZ edge and in the SCM at Station 2; on the OMZ edge, in the SCM, and in the SNM at
493 Station 3; in the SNM at Station 3.5; and on the OMZ edge at Station 4. For each experiment, a
494 total of 24 bottles were filled with water collected at a specific depth, sealed with deoxygenated
495 stoppers, and then bubbled with ultrapure He gas (15-30 minutes) while DO was monitored. We
496 introduced an He headspace of 20 mL, and air was injected into bottles to raise DO
497 concentrations when needed. For each experiment, we established initial DO values ranging
498 from 10s to 1000s of nM (Figure 4), and 8 bottles had tracer-level $^{15}NO_2^-$ additions, 8 bottles had
499 tracer-level $^{15}NH_4^+$ additions, and 8 were unlabeled. For all experiments and water column
500 profiles, bottles were cleaned with 0.1 M HCl and triple rinsed with water between incubations,
501 and dedicated bottles were used for the different ^{15}N labels.
502 OCR was measured in all experimental bottles based on starting and ending DO values,
503 and samples for nitrite oxidation were collected from $^{15}NO_2^-$ labeled bottles at the end of the
504 experiments. Four to eight bottles in each experiment were also continuously monitored for DO
505 concentration changes throughout the experiment. We tested DO consumption curves for
506 linearity over time using the Maximal Information Coefficient (MIC; ref. 59) and linear
507 regression. MIC effectively captures both linear and nonlinear relationships, such that

508 differences between higher MIC scores and lower regression coefficients are indicative of
509 nonlinear relationships, whereas high MIC scores combined with high r^2 values are indicative of
510 strong linear relationships[59]. We found the vast majority of DO time courses were linear (r^2 >0.6,
511 MIC-r^2 <0.2). The few exceptions—one incubation bottle each in the SCM at Stations 2 and 3,
512 one in the SNM at Station 3, two in the SNM at Station 3.5, and one on the OMZ edge at Station
513 4—all showed a decline in OCR over time. All of these incubation bottles had average DO <235
514 nM, and were used to calculate affinity for DO at these low concentrations (Supplementary Note
515 1).
516
517 **Nitrate isotopic measurements.** Both natural abundance and ^{15}N-tracer-based nitrate isotopes
518 were quantified by use of the denitrifier method[60,61]. Samples were collected from the rosette or
519 at the end of incubations, filtered through a 0.2 μm filter, and then frozen until analysis. In the
520 lab, 20-30 nmoles of NO_3^- were quantitatively converted to N_2O by a culture of the denitrifying
521 bacterium, *Pseudomonas aureofaciens*. Product N_2O was cryogenically purified and trapped
522 under flow of ultra-high purity He, before being introduced to an IsoPrime 100 isotope ratio
523 mass spectrometer. Isotope ratios were normalized to international reference materials (USGS
524 32, USGS 34, USGS 35) and reported using standard delta notation. Any nitrite present in the
525 sample was removed by addition of sulfamic acid[37]. In samples from the upper 100 m, where
526 NO_3^- concentrations were low, 'carrier' NO_3^- of known isotopic composition was added and
527 sample compositions were calculated by mass balance. Precision of natural abundance isotope
528 ratio measurements was ±0.3‰ and ±0.4‰ for δ^{15}N and δ^{18}O, respectively. δ^{15}N and δ^{18}O
529 values were used to calculate the Δ(15,18) deviation from the 1:1 line following Sigman et al.[41].
530
531 **Nitrite Oxidation Rates.** Nitrite oxidation rates were measured by adding 98 atom percent
532 (atom%) $^{15}NO_2^-$ to a final concentration of 12-184 nmol L^{-1}—representing 5-10% of *in situ* NO_2^-
533 concentrations (with the exception of some samples in the upper 100m with no measurable
534 nitrite)—and measuring the accumulation of ^{15}N label in the NO_3^- pool following Beman et al.[7].
535 After incubation for ~24 hours, samples were frozen at sea. Upon thawing in the laboratory,
536 excess $^{15}NO_2^-$ was removed following Granger and Sigman[37]. In brief, sulfamic acid (~8-10 μL
537 mL^{-1}) was added, the samples were shaken and allowed to sit for >5 minutes, and then samples
538 were neutralized by adding NaOH (4 M, ~11 μL mL^{-1}) prior to analysis.

539 Rates of $^{15}NO_2^-$ oxidation ($^{15}R_{ox}$) were calculated using equation 1 from Beman et al.[7]
540 adapted from Ward et al. (ref. 62):

541 $$^{15}R_{ox} = \frac{\left(n_t - n_{oNO_3^-}\right) \times \left[NO_3^-\right]}{\left(n_{NO_2^-}\right) \times t} \quad (1)$$

542 where n_t is the atom% ^{15}N in NO_3^- measured at time t corrected for $^{15}NO_3^-$ contamination of the
543 $^{15}NO_2^-$ stock; $n_{oNO_3^-}$ is the measured atom% ^{15}N of unlabeled NO_3^-; $[NO_3^-]$ is the concentration of
544 the NO_3^- pool; and $n_{NO_2^-}$ is the exponential average atom% of NO_2^- over time t. $n_{NO_2^-}$ was
545 calculated by isotope mass balance based on initial NO_2^- concentrations, measured isotopic
546 composition, added ^{15}N-labeled NO_2^-, and measured $^{15}NH_4^+$ oxidation rates (which produce
547 unlabeled NO_2^-; ammonia oxidation rate measurements followed Beman et al.[30]).
548
549 **RNA/DNA Extractions, 16S rRNA Sequencing and Analysis, Metagenome Sequencing and**
550 **Analysis, and Organic Matter Analysis** are reported in the Supplementary Materials and
551 Methods.
552
553 **Sequence data** are available in the Sequence Read Archive under BioProjects PRJNA192803
554 (16S data), and PRJNA634212 (metagenomes).
555
556 **Statistical analyses** were carried out in the R statistical environment (RStudio Version 1.0.136).
557 Linear regressions were performed using the 'lm' function in R; Michaelis-Menten curve fits
558 (Supplementary Note 2) were performed using the 'drm' function in the R package drc (ref. 63).
559
560 **Acknowledgments**
561 This work was supported by NSF CAREER grant OCE-1555375 to J.M.B. Metagenome
562 sequencing was supported by the UCMEXUS-CONACyT Collaborative Grants Program (to
563 J.M.B. and José García Maldonado). We thank the officers and crew of the *R/V Oceanus* for
564 their help at sea, and thank Sarah Abboud, Daniela Alonso, DeVonyo Bills, Jorge Montiel
565 Molina, and Kevin Testo for their assistance in the field.
566
567 **References**

1. M. G. Pachiadaki, *et al.*, Major role of nitrite-oxidizing bacteria in dark ocean carbon fixation. *Science* **358**, 1046–1051 (2017).
2. M. A. Saito, *et al.*, Abundant nitrite-oxidizing metalloenzymes in the mesopelagic zone of the tropical Pacific Ocean. *Nat. Geosci.* **13**, 355–362 (2020).
3. C. A. Francis, J. M. Beman, M. M. M. Kuypers, New processes and players in the nitrogen cycle: The microbial ecology of anaerobic and archaeal ammonia oxidation. *ISME J.* **1**, 19–27 (2007).
4. A. D. Bertagnolli, F. J. Stewart, Microbial niches in marine oxygen minimum zones. *Nat. Rev. Microbiol.* **16**, 723–729 (2018).
5. B.B. Ward, "Nitrification in Marine Systems" in Nitrogen in the Marine Environment, 2nd Ed., D. Capone, D. Bronk, M. R. Mulholland, E. Carpenter, Eds. (Elsevier Inc., 2008), pp. 199-263.
6. J. Füssel, *et al.*, Nitrite oxidation in the Namibian oxygen minimum zone. *ISME J.* **6**, 1200–1209 (2012).
7. J. M. Beman, J. Leilei Shih, B. N. Popp, Nitrite oxidation in the upper water column and oxygen minimum zone of the eastern tropical North Pacific Ocean. *ISME J.* **7**, 2192-2205 (2013) https:/doi.org/10.1038/ismej.2013.96.
8. X. Peng, *et al.*, Ammonia and nitrite oxidation in the Eastern Tropical North Pacific. *Global Biogeochem. Cycles* **29**, 2034–2049 (2015).
9. X. Sun, Q. Ji, A. Jayakumar, and B.B Ward, Dependence of nitrite oxidation on nitrite and oxygen in low-oxygen seawater. *Geophysical Res. Lett.* **44**, 7883-7891 (2017).
10. A. Paulmier, D. Ruiz-Pino, Oxygen minimum zones (OMZs) in the modern ocean. *Prog. Oceanogr.* **80**, 113–128 (2009).
11. O. Ulloa, D. E. Canfield, E. F. DeLong, R. M. Letelier, F. J. Stewart, Microbial oceanography of anoxic oxygen minimum zones. *Proc. Natl. Acad. Sci. U. S. A.* **109**, 15996–16003 (2012).
12. B. Thamdrup, T. Dalsgaard, N. P. Revsbech, Widespread functional anoxia in the oxygen minimum zone of the Eastern South Pacific. *Deep. Res. Part I Oceanogr. Res. Pap.* **65**, 36–45 (2012).
13. D. Tsementzi, *et al.*, SAR11 bacteria linked to ocean anoxia and nitrogen loss. *Nature* **536**, 179–183 (2016).

14. A. R. Babbin, R. G. Keil, A. H. Devol, B. B. Ward, Organic matter stoichiometry, flux, and oxygen control nitrogen loss in the ocean. *Science* **344**, 406–408 (2014).
15. E. Garcia-Robledo, *et al.*, Cryptic oxygen cycling in anoxic marine zones. *Proc. Natl. Acad. Sci. U. S. A.* **114**, 8319–8324 (2017).
16. L. Tiano, Laura, *et al.*, Oxygen distribution and aerobic respiration in the north and south eastern tropical Pacific oxygen minimum zones. *Deep Sea Re.s Part I: Oceanogr. Res. Papers* **94**: 173-183 (2014).
17. J. L. Penn, T. Weber, B. X. Chang, C. Deutsch, Microbial ecosystem dynamics drive fluctuating nitrogen loss in marine anoxic zones. *Proc. Natl. Acad. Sci. U. S. A.* **116**, 7220–7225 (2019).
18. T. Kalvelage, *et al.*, Aerobic Microbial Respiration In Oceanic Oxygen Minimum Zones. *PLoS One* **10**, e0133526 (2015).
19. E. Garcia-Robledo, *et al.*, Determination of respiration rates in water with sub-micromolar oxygen concentrations. *Front. Mar. Sci.* 3: 244 (2016).
20. R. Goericke, R. J. Olson, A. Shalapyonok, A novel niche for Prochlorococcus sp. in low-light suboxic environments in the Arabian Sea and the Eastern Tropical North Pacific. *Deep. Res. Part I Oceanogr. Res. Pap.* **47**, 1183–1205 (2000).
21. P. Lavin, B. González, J. F. Santibáñez, D. J. Scanlan, O. Ulloa, Novel lineages of Prochlorococcus thrive within the oxygen minimum zone of the eastern tropical South Pacific. *Environ. Microbiol. Rep.* **2**, 728–738 (2010).
22. L. A. Bristow, *et al.*, Ammonium and nitrite oxidation at nanomolar oxygen concentrations in oxygen minimum zone waters. *Proc. Natl. Acad. Sci. U. S. A.* **113**, 10601–10606 (2016).
23. T. Kalvelage, *et al.* Oxygen sensitivity of anammox and coupled N-cycle processes in oxygen minimum zones. *PloS ONE* 6.12: e29299 (2011).
24. X. Sun, *et al.*, Microbial niche differentiation explains nitrite oxidation in marine oxygen minimum zones. *ISME J.* (2021).
25. H. Daims, S. Lücker, M. Wagner, A New Perspective on Microbes Formerly Known as Nitrite-Oxidizing Bacteria. *Trends Microbiol.* **24**, 699–712 (2016).
26. X. Sun, *et al.*, Uncultured Nitrospina-like species are major nitrite oxidizing bacteria in oxygen minimum zones. *ISME J.* **13**, 2391–2402 (2019).

27. A.R. Babbin, *et al.* Nitrite oxidation exceeds reduction and fixed nitrogen loss in anoxic Pacific waters. *Marine Chemistry* **224**: 103814 (2020).

28. J. Füssel, *et al.*, Adaptability as the key to success for the ubiquitous marine nitrite oxidizer Nitrococcus. *Sci. Adv.* **3**, e1700807 (2017).

29. P. Lam, *et al.*, Revising the nitrogen cycle in the Peruvian oxygen minimum zone. *Proc. Natl. Acad. Sci. U. S. A.* **106**, 4752-7 (2009).

30. J. M. Beman, B. N. Popp, S. E. Alford, Quantification of ammonia oxidation rates and ammonia-oxidizing archaea and bacteria at high resolution in the Gulf of California and eastern tropical North Pacific Ocean. *Limnol. Oceanogr.* **57**, 711–726 (2012).

31. F. Lipschultz, *et al.*, Bacterial transformations of inorganic nitrogen in the oxygen-deficient waters of the Eastern Tropical South Pacific Ocean. *Deep Sea Res. Part A, Oceanogr. Res. Pap.* **37**, 1513–1541 (1990).

32. M. Holtappels, *et al.*, Aquatic respiration rate measurements at low oxygen concentrations. *PLoS One* **9** (2014).

33. P. Lehner, *et al.*, LUMOS - A sensitive and reliable optode system for measuring dissolved oxygen in the nanomolar range. *PLoS One* **10**, 1–15 (2015).

34. W. F. Gilly, J. M. Beman, S. Y. Litvin, B. H. Robison, Oceanographic and Biological Effects of Shoaling of the Oxygen Minimum Zone. *Ann. Rev. Mar. Sci.* **5**, 393–420 (2013).

35. J. Granger, S. D. Wankel, Isotopic overprinting of nitrification on denitrification as a ubiquitous and unifying feature of environmental nitrogen cycling. *Proc. Natl. Acad. Sci. U. S. A.* **113**, E6391–E6400 (2016).

36. K. L. Casciotti, Nitrogen and Oxygen Isotopic Studies of the Marine Nitrogen Cycle. *Ann. Rev. Mar. Sci.* **8**, 379–407 (2016).

37. J. Granger J and D.M. Sigman. Removal of nitrite with sulfamic acid for nitrate N and O isotope analysis with the denitrifier method. *Rapid Commun. Mass Spectrom.* **23**, 3753–3762 (2009).

38. L. A. Treibergs, J. Granger, Enzyme level N and O isotope effects of assimilatory and dissimilatory nitrate reduction. *Limnol. Oceanogr.* **62**, 272–288 (2017).

39. C. Buchwald, K. L. Casciotti, Oxygen isotopic fractionation and exchange during bacterial nitrite oxidation. *Limnol. Oceanogr.* **55**, 1064–1074 (2010).

40. T. C. Hollocher, Source of the oxygen atoms of nitrate in the oxidation of nitrite by Nitrobacter agilis and evidence against a PON anhydride mechanism in oxidative phosphorylation. *Arch. Biochem. Biophys.* **233**, 721–727 (1984).

41. D. M. Sigman, *et al.*, Coupled nitrogen and oxygen isotope measurements of nitrate along the eastern North Pacific margin. *Global Biogeochem. Cycles* **19**, GB4022 (2005).

42. K. L. Casciotti, M. R. McIlvin, Isotopic analyses of nitrate and nitrite from reference mixtures and application to Eastern Tropical North Pacific waters. *Mar. Chem.* **107**, 184–201 (2007).

43. B. J. Callahan, *et al.*, DADA2: High-resolution sample inference from Illumina amplicon data. *Nat. Methods* **13**, 581–583 (2016).

44. J. J. Wright, K. M. Konwar, S. J. Hallam, Microbial ecology of expanding oxygen minimum zones. *Nat. Rev. Microbiol.* **10**, 381–394 (2012).

45. S. Lücker, B. Nowka, T. Rattei, E. Spieck, H. Daims, The genome of Nitrospina gracilis illuminates the metabolism and evolution of the major marine nitrite oxidizer. *Front. Microbiol.* **4**, 27 (2013).

46. M. Larsen, *et al.* In situ quantification of ultra-low O_2 concentrations in oxygen minimum zones: Application of novel optodes. *Limnology and Oceanography: Methods* **14**: 784-800 (2016).

47. K. F. Ettwig, *et al.*, Nitrite-driven anaerobic methane oxidation by oxygenic bacteria. *Nature* **464**, 543–548 (2010).

48. B. Thamdrup, *et al.*, Anaerobic methane oxidation is an important sink for methane in the ocean's largest oxygen minimum zone. *Limnol. Oceanogr.* **64**, 2569–2585 (2019).

49. D. E. Canfield, *et al.*, A Cryptic Sulfur Cycle in Oxygen-Minimum-Zone Waters off the Chilean Coast. *Science* **330**, 1375–1378 (2010).

50. F. J. Pavia, *et al.*, Shallow particulate organic carbon regeneration in the South Pacific Ocean. *Proc. Natl. Acad. Sci. U. S. A.* **116**, 9753–9758 (2019).

51. D. A. Stolper, N. P. Revsbech, D. E. Canfield, Aerobic growth at nanomolar oxygen concentrations. *Proc. Natl. Acad. Sci. U. S. A.* **107**, 18755–18760 (2010).

52. R. L. Morris, T. M. Schmidt, Shallow breathing: Bacterial life at low O 2. *Nat. Rev. Microbiol.* **11**, 205–212 (2013).

53. E. J. Zakem, M. J. Follows, A theoretical basis for a nanomolar critical oxygen concentration. *Limnol. Oceanogr.* **62**, 795–805 (2017).

54. C. Deutsch, H. Brix, T. Ito, H. Frenzel, L. A. Thompson, Climate-forced variability of ocean hypoxia. *Science* **333**, 336–339 (2011).

55. S. Ganesh, *et al.*, Size-fraction partitioning of community gene transcription and nitrogen metabolism in a marine oxygen minimum zone. *ISME J.* 9: 2682-2696 (2015).

56. J.M. Beman, J.M. and M.T. Carolan, Deoxygenation alters bacterial diversity and community composition in the ocean's largest oxygen minimum zone. *Nature Comm.* **4**, 1-11 (2013).

57. E.J. Zakem, A. Mahadevan, J.M. Lauderdale, M.J. Follows, Stable aerobic and anaerobic coexistence in anoxic marine zones. *ISME J.* **14**, 288-301 (2020).

58. J. M. Wilson, S. Y. Litvin, J. M. Beman, Microbial community networks associated with variations in community respiration rates during upwelling in nearshore Monterey Bay, California. *Environ. Microbiol. Rep.* **10**, 272–282 (2018).

59. D.N. Reshef, *et al.*, Detecting novel associations in large data sets. *Science* 334: 1518-1524 (2011).

60. K. L. Casciotti, D. M. Sigman, M. G. Hastings, J. K. Böhlke, A. Hilkert, Measurement of the oxygen isotopic composition of nitrate in seawater and freshwater using the denitrifier method. *Anal. Chem.* **74**, 4905–4912 (2002).

61. D. M. Sigman, *et al.*, A bacterial method for the nitrogen isotopic analysis of nitrate in seawater and freshwater. *Anal. Chem.* **73**, 4145–4153 (2001).

62. B. B. Ward, K. A. Kilpatrick, E. H. Renger, R. W. Eppley, Biological nitrogen cycling in the nitracline. *Limnol. Oceanogr.* **34**, 493–513 (1989).

63. C. Ritz, F. Baty, J. C. Streibig, D. Gerhard, Dose-response analysis using R. *PLoS One* **10** (2015).

Figures (for initial submission)

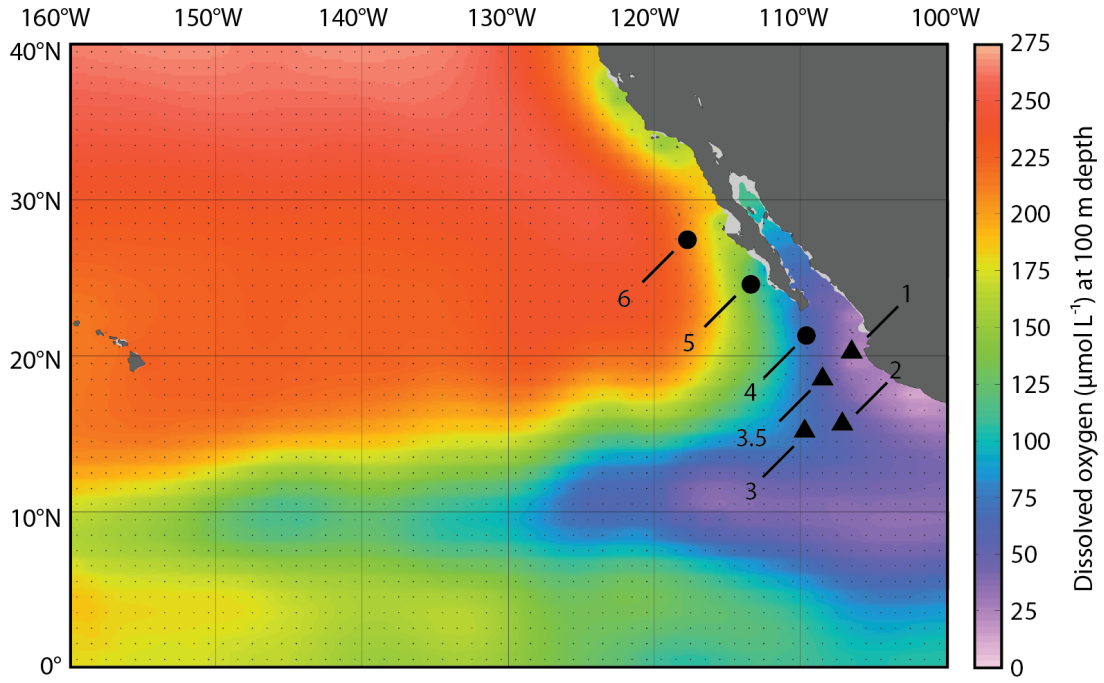

Figure 1: Station locations (numbered symbols) in the ETNP plotted on dissolved oxygen concentrations (in µM) at 100 m depth from the World Ocean Atlas. Triangles denote AMZ Stations 1-3.5 and circles denote OMZ stations 4-6.

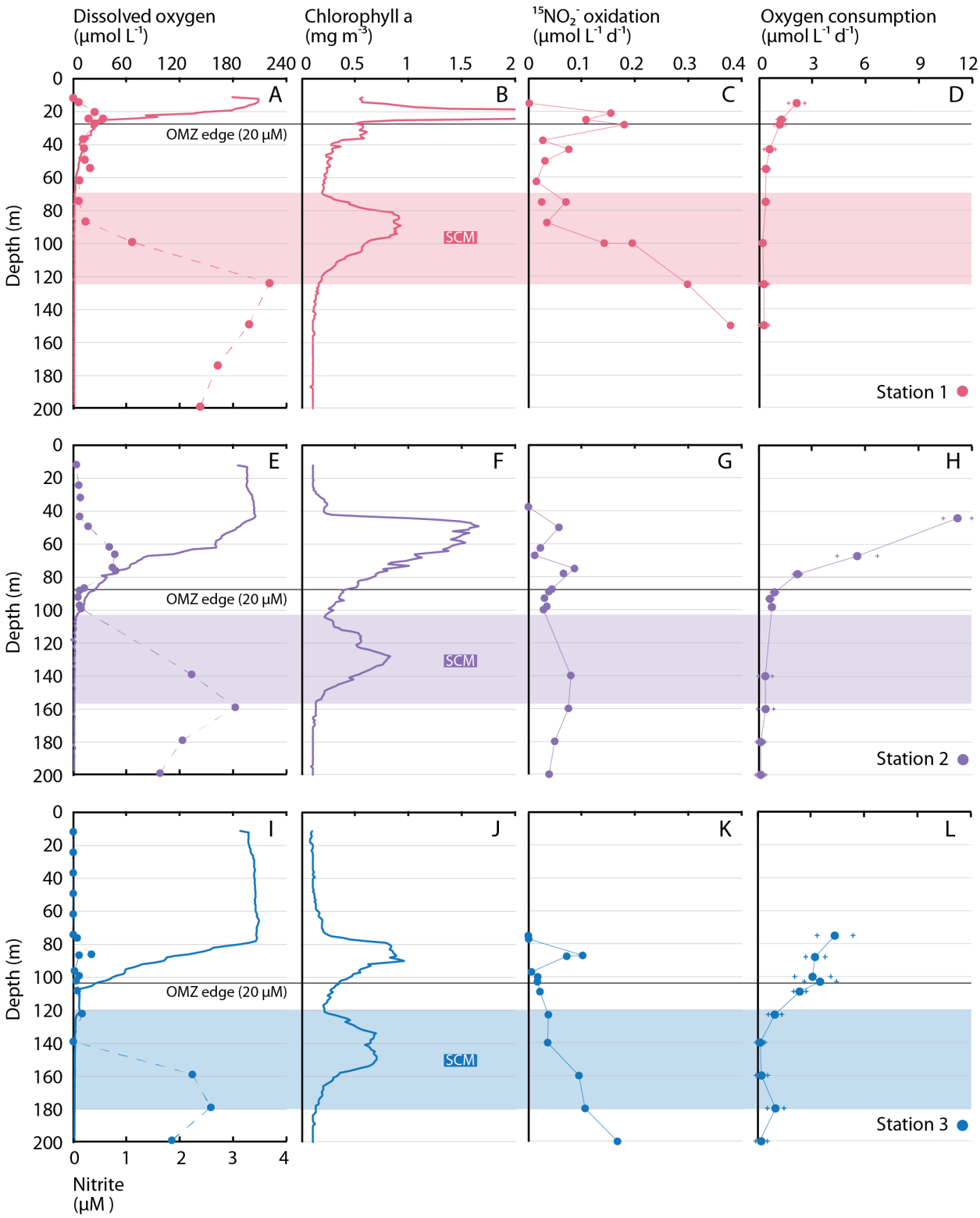

Figure 2: Depth profiles of (A,E,I) DO (solid lines) and nitrite (data points connected by dashed lines), (B,F,J) chlorophyll a, (C,G,K) nitrite oxidation rates, and (D,H,L) OCR (error bars denote

standard deviation of five replicates) show consistent variation across (A-D) Station 1, (E-H) Station 2, and (I-L) Station 3 (denoted by different colors). Black horizontal lines denote the depth of the OMZ, and shaded areas show the SCM at each station. Rates measured below the SCM should be considered potential rates (see main text). Maximum chlorophyll values at Station 1 plot off-axis.

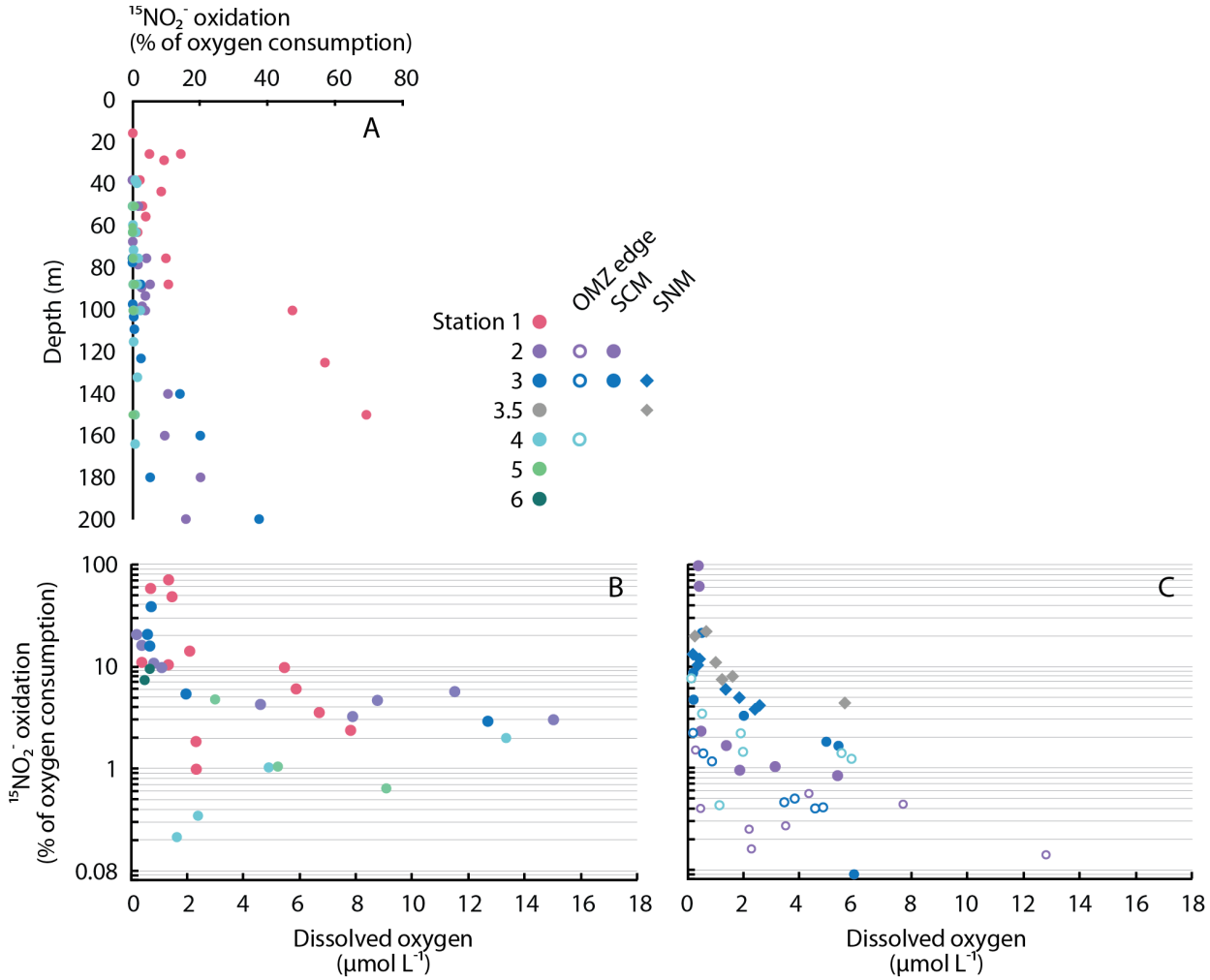

Figure 3: DO consumption via nitrite oxidation as a percentage of OCR with (A) depth, and as a function of average DO in (B) depth profiles and (C) oxygen manipulation experiments. Colors denote different stations. Only measurements for DO <18 µM are included in panel B, and all experimental bottles with dual nitrite oxidation and OCR are shown in C. In panel C, different symbols denote experiments conducted in different regions of the water column, with two

experiments conducted at Station 2 (OMZ edge, open purple circles; SCM, filled purple circles), three at Station 3 (OMZ edge, open blue circles; SCM, filled blue circles; SNM, blue diamonds), and one each at Stations 3.5 (SNM, grey diamonds) and 4 (OMZ edge, open light blue circles).

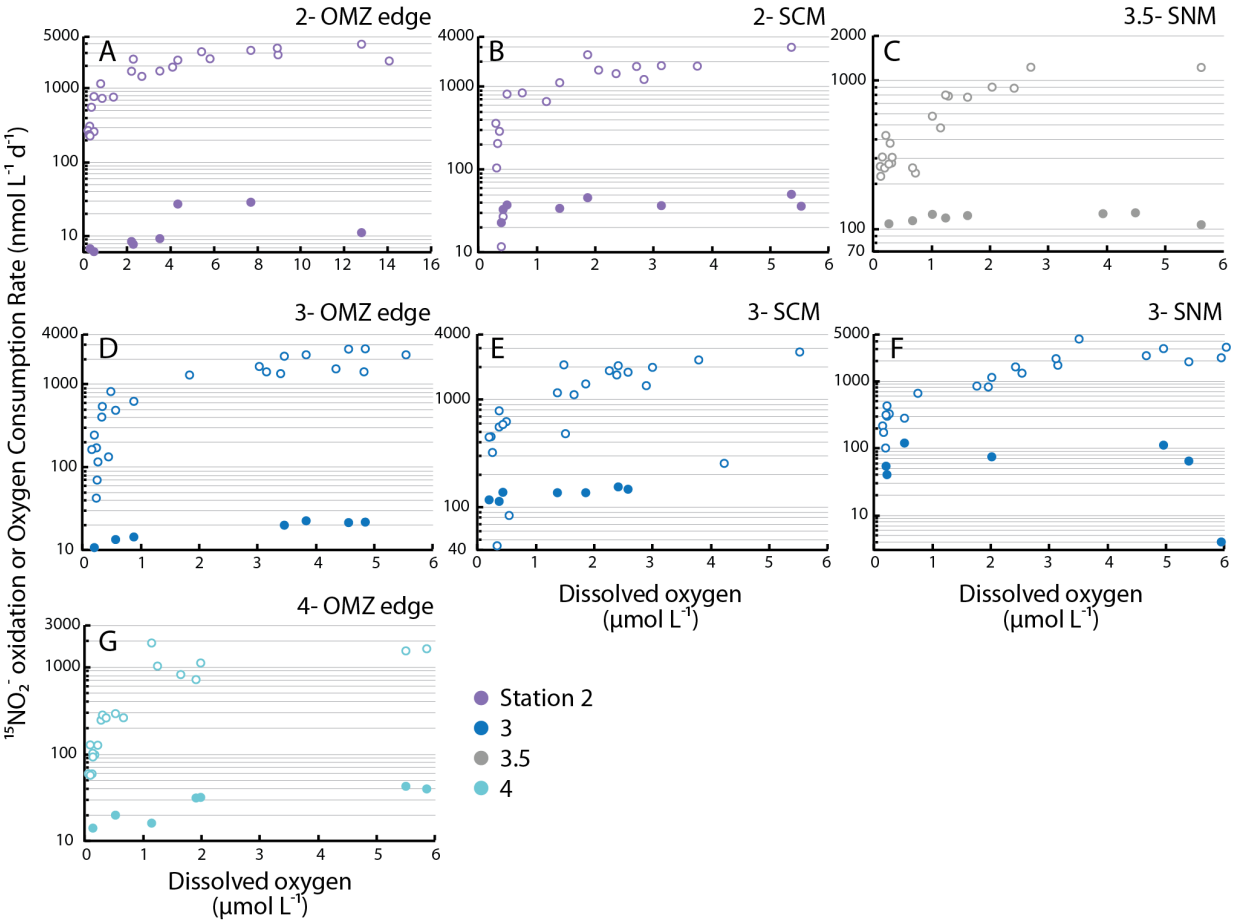

Figure 4: Nitrite oxidation rates (filled symbols) and OCR (open symbols) as a function of average DO in oxygen manipulation experiments. Colors denote different stations, with panels displaying data from different experiments: A) Station 2 OMZ edge (20 µM DO), B) Station 2 SCM, C) Station 3.5 SNM, D) Station 3 OMZ edge, E) Station 3 SCM, F) Station 3 SNM, and G) Station 4 OMZ edge. Note differences in vertical axes between experiments, and differences in horizontal axis in panel A compared with the remaining panels.

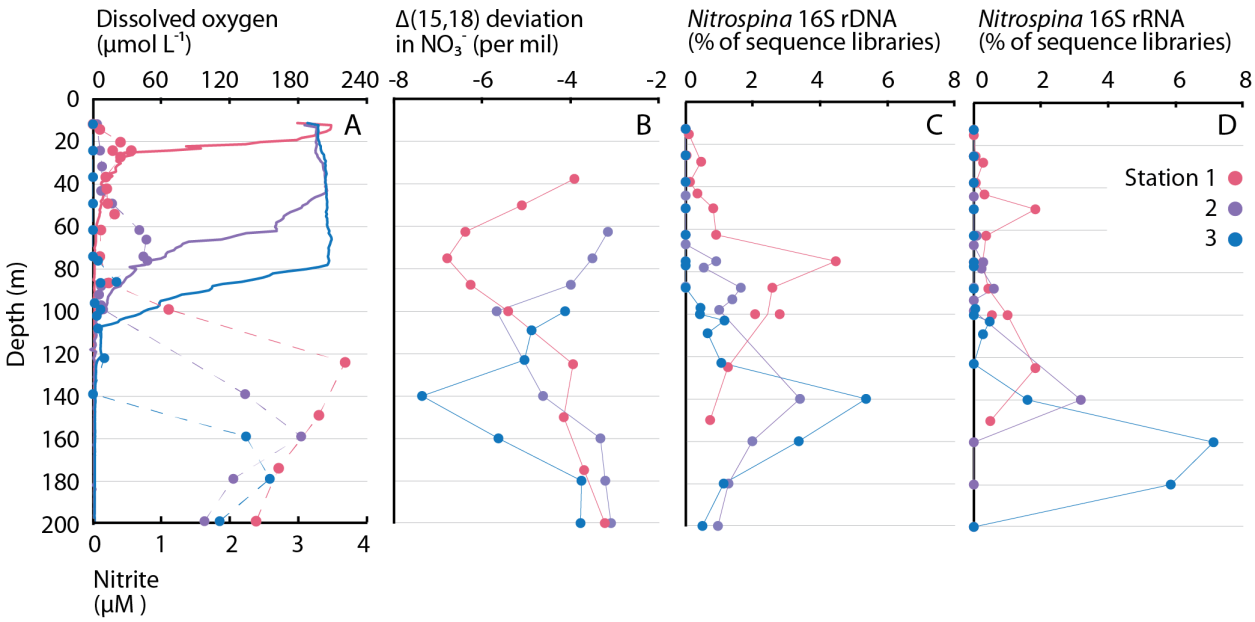

Figure 5: Depth profiles of (A) DO (solid lines) and nitrite (data points connected by dashed lines), (B) Δ(15,18) dual-isotope deviations in nitrate, and *Nitrospina* ASVs as a percentage of (C)16S rDNA sequence libraries and (D) 16S rRNA sequence libraries. Colors denote different sampling stations.

Table 1: Details of oxygen manipulation experiments, including: station, sampling depth, region of the water column, and experiment length; initial DO measured using oxygen sensor spots (FireSting) prior to experimental manipulation, total organic carbon (TOC), and nitrite concentrations; and calculated parameters for OCR (including both low-level and overall K_m values) and nitrite oxidation rates (K_m values are for dissolved oxygen in all cases, with ±standard error shown). NA=not applicable, and NS=parameter estimate not significant.

Experiment	**2-1**	**2-2**	**3-1**	**3-2**	**3-3**	**3.5-1**	**4-1**
Station	2	2	3	3	3	3.5	4
Depth (m)	90	140	130	170	110	80	100
Region of the water column	OMZ edge	SCM	SCM	SNM	OMZ edge	SNM	OMZ edge
Length (hr)	22	19	16	16	22	17	24
Initial DO (nM)	19940	480	293	260	12800	274	3480
TOC (nM)	57965	45318	49118	46929	51211	44339	47397*
Nitrite (nM)	203	205	100	2410	73	2650	68
OCR							
Low-level K_m (nM)	NA	124	127	81	NA	53-104	82
Overall K_m (nM)	3262 ±930	1787 ±689	1804 ±117	NS	NS	1621 ±546	1738 ±755
v_{max} (nmol L^{-1} d^{-1})	4164 ±457	2757 ±1146	2765 ±788	5973 ±2217	4025 ±1247	1612 ±262	2075 ±415
r^2	.878	.811	.569	.757	.868	.846	.776
Nitrite oxidation							
Overall K_m (nM)	NS	185 ±88	63.8 ±24.2	NS	346 ±95	34.1 ±15.0	1015 ±614
v_{max} (nmol L^{-1} d^{-1})	NS	43.9 ±4.2	149 ±6	71.2 ±21.8	23.0 ±1.2	122 ±4	47.5 ±8.6
r^2	.347	.445	.665	.019	.910	.269	.825

*Station 4 TOC sample was collected at 90 m

772 **Table 2:** Relative abundance of *Nitrospina* reads, functional genes from *Nitrospina*, and
773 *Prochlorococcus* reads within metagenomes (expressed per million reads) collected on the edge
774 of the OMZ, in the SCM, and in the SNM at Stations 1-3.
775

Sta.	Depth	Depth region	Initial DO (µM)	*Nitrospina* (all reads)	*Nitrospina* Nitrite oxido-reductase (*nxr*)	*Nitrospina* Cyto-chrome *c* oxidase	*Nitrospina* Cyto-chrome *bd* oxidase	*Prochloro-coccus* (all reads)
1	25	OMZ edge	19.9	1084	2	0	0	865
1	87.5	SCM	0.46	31920	65	20	3	47992
1	100	SNM	0.30	21196	37	22	2	10765
2	89	OMZ edge	15.3	22442	38	12	10	57194
2	130	SCM	0.78	33290	57	20	4	33522
2	160	SNM	0.60	21725	37	28	2	4157
3	123	OMZ edge	13.0	18647	34	10	2	54709
3	140	SCM	0.74	34227	55	18	4	37202
3	180	SNM	0.45	17617	30	26	2	4881

776 Initial DO concentrations were measured in unmanipulated incubation bottles using oxygen
777 sensor spots (Fibox) immediately following sample collection.